

# Decrease in Photovoltaic Power Output from Ripple: Simple General Calculation and the Effect of Partial Shading

Charles R. Sullivan, *Senior Member, IEEE*, Jonathan J. Awerbuch, and Alexander M. Latham, *Member, IEEE*

**Abstract**—The effect of voltage ripple on the power output of a photovoltaic panel is calculated and tested experimentally. Voltage ripple induces a much larger power reduction than would be predicted from a conventional small-signal model of the panel's  $I$ - $V$  characteristic, even with small ripple amplitude. A simple expression is provided to calculate power reduction from rms ripple voltage, for any ripple waveform shape. The effect of ripple on power output can be much more severe under nonuniform irradiance as can result from partial shading. The results are important for

- 1) consideration of double-line-frequency ripple in single-phase inverters;
- 2) high-frequency switching ripple with any power converter in a photovoltaic system; and
- 3) perturbations and tracking errors in maximum-power-point tracking systems.

**Index Terms**—Maximum-power-point tracking (MPPT), photovoltaics, ripple, single-phase inverter.

## I. INTRODUCTION

IT is well known that the output of a photovoltaic (PV) cell or panel is maximized by operating at a specific point on its exponential voltage-current characteristic curve, the maximum power point (MPP). Because the MPP varies with temperature and irradiance, maximum power point tracking (MPPT) systems (surveyed in [1] and [2]) are commonly used in order to operate the panel at this point. However, the voltage and current on the panel are rarely purely dc—various ripple components and deliberate or accidental control perturbations produce temporary, minor deviations from the MPP. Understanding the impact of these excursions away from the MPP is essential for rational design of high-performance systems for extracting maximum energy from PV panels. This includes sizing high-frequency filter components in switching converters and invert-

ers, energy buffering in single-phase inverters [3]–[11], and designing MPPT systems to minimize perturbation size [12] or the combined effect of algorithmic and noise-induced perturbations [13], [14].

An intuitively appealing approach to estimating the reduction in power output due to ripple would be to derive a small-signal model by fitting a tangent line to the  $I$ - $V$  curve at the MPP, and then calculate power reduction from the linearized model, which results in

$$P_{ss} = I_{\text{ripple,rms}}^2 R_{ss} = V_{\text{ripple,rms}}^2 / R_{ss} \quad (1)$$

where  $R_{ss}$  is the small-signal resistance. However, the actual power reduction is much larger than would be estimated by this simple small-signal approach. The larger reduction in power is described in [3], analyzed in [15]–[17], and experimentally verified in [16] and [17].

One might expect that the larger power reduction compared to that predicted from (1) would vanish as the size of the perturbation was reduced—that with sufficiently small ripple the small-signal model would become valid, and so would (1). However, (1) neglects a term that dominates the power reduction even with arbitrarily small ripple. This can be shown through a Taylor-series expansion of the PV panel output power [3], [15].

This paper provides a simple, practical formulation of the reduction in power output arising from ripple and other perturbations. It is easier to use and more generally applicable, especially in contrast to the Bessel-function analysis of a sinusoidal ripple in [16], and does not require simulations [7], [8] or experimental measurements [5]. The calculation requires only the rms value of the voltage ripple, independent of the shape of the ripple waveform. The power reduction is typically nearly an order of magnitude higher than would be predicted by (1). In addition, the paper discusses the effect of nonuniform irradiance on the different cells of a PV panel, and shows that in this case, the effect of ripple can be dramatically magnified. The power reduction effect of ripple is experimentally verified for a range of ripple amplitudes, frequencies, and waveforms.

The large effect of ripple on power output has important implications for the design of single-phase inverters, which require large capacitors, active buffering, or both to avoid excessive double-line-frequency ripple on the panel [3]–[11]. In a three-phase or dc application, the implication is that switching-frequency ripple should be stringently filtered. In MPPT algorithms, the importance of accurate tracking and small perturbations is emphasized; as perturbations are reduced in order to reduce ripple-induced power reduction, noise becomes more

Manuscript received January 2, 2012; revised April 2, 2012; accepted May 28, 2012. Date of current version September 27, 2012. This work was supported in part by the National Science Foundation under Grant ECCS-0925280. Recommended for publication by Associate Editor T. Shimizu.

C. R. Sullivan is with the Thayer School of Engineering at Dartmouth, Hanover, NH 03755 USA (e-mail: charles.r.sullivan@dartmouth.edu).

J. J. Awerbuch is with the Department of Mechanical Engineering, University of Colorado at Boulder, Boulder, CO 80309 USA (e-mail: j.awerbuch@gmail.com).

A. M. Latham is with Thayer School of Engineering at Dartmouth, Hanover, NH 03755 USA, and also with the Allegro Microsystems, Manchester, NH 03103 USA (e-mail: alexander.latham@gmail.com).

Color versions of one or more of the figures in this paper are available online at <http://ieeexplore.ieee.org>.

Digital Object Identifier 10.1109/TPEL.2012.2205162

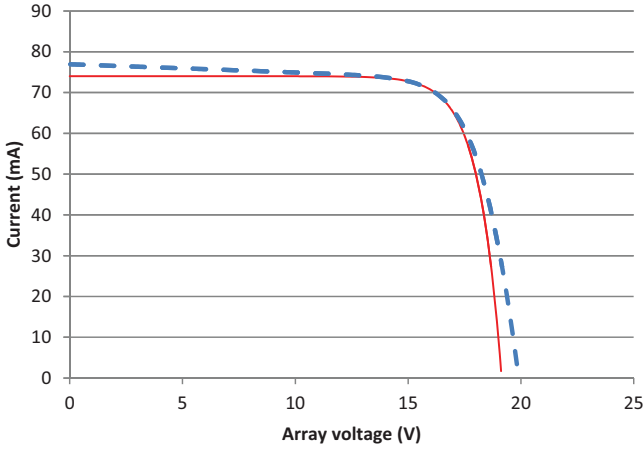


Fig. 1. Comparison of two models for a solar array, showing that there is no significant difference in the region of interest near the MPP. The solid line is the simple diode model given by (2); the dashed line is for a model with shunt and series resistances of 5 k $\Omega$  and 10  $\Omega$ , respectively. This shows that the simple diode model is adequate.

prominent, and balancing the effects of noise and perturbations becomes important for achieving high performance [13], [14]. The results also help quantify the benefits of using inherent ripple from the operation of the power conversion hardware for MPPT, without deliberately introducing additional perturbations [5], [18]–[20].

## II. ANALYSIS

A simple exponential diode model of a solar panel with identical cells with identical irradiance and temperature is used for analysis [21]

$$i(t) = I_{sc} - I_s \left( e^{\frac{v(t)}{n m V_T}} - 1 \right) \quad (2)$$

where  $i(t)$  is the panel current,  $v(t)$  is the panel voltage,  $m$  is the number of cells,  $I_{sc}$  is the short-circuit current (proportional to irradiance),  $V_T$  is thermal voltage, and  $I_s$  and  $n$  are diode characteristic parameters (scale current and ideality factor, respectively). The physics behind the model is described in, for example, [22]. Although more sophisticated models are available [21], [22], the shape near the knee of the curve, where the MPP is located, is captured well by this simple model. For example, Fig. 1 compares the simple diode model (2) to a common model with shunt and series resistors [22]. The models can be seen to provide virtually identical behavior in the region of interest near the MPP. Thus, the simple diode model (2) is appropriate for this study.

For high-frequency ripple, the capacitance of the diode may also be important. As in [16], the effect of parallel capacitance can be considered separately from the analysis of power reduction due to ripple by defining the variable  $i(t)$  to be exclusive of the current through the capacitance. The terminal voltage is equal to the variable  $v(t)$  with or without capacitance, so the results are most directly applicable when formulated in terms of ripple voltage. If they are written in terms of ripple current, an additional correction for capacitance is necessary at high frequency.

Panel output power is simply the product of panel voltage and current, and can be written in terms of  $v(t)$

$$P = v(t)I_{sc} - v(t)I_s \left( e^{\frac{v(t)}{n m V_T}} - 1 \right). \quad (3)$$

The power near an operating point,  $(V_0, I_0)$ , can be approximated by a Taylor expansion of  $P(v(t))$

$$p(t) \approx V_0 I_0 + \Delta v(t) \frac{dP}{dv} + \frac{1}{2} \Delta v(t)^2 \frac{d^2 P}{dv^2} \quad (4)$$

where  $\Delta v(t)$  is the instantaneous deviation from the voltage at the operating point  $V_0$ .

At the MPP  $(V_{mp}, I_{mp})$ , the first derivative  $dP/dv = 0$ , and so the first-order term in (4) is zero, such that

$$p(t) \approx V_{mp} I_{mp} + \frac{1}{2} \Delta v(t)^2 \frac{d^2 P}{dv^2}. \quad (5)$$

The time-average reduction in power harvested can be written in terms of the rms value of voltage ripple,  $(\Delta v)_{rms}$ , as

$$P_r \approx -\frac{1}{2} ((\Delta v)_{rms})^2 \frac{d^2 P}{dv^2}. \quad (6)$$

Substituting the second derivative of (3), as detailed in Appendix A, results in

$$P_r \approx ((\Delta v)_{rms})^2 \frac{1}{R_{ss}} \left( 1 + \frac{V_{mp}}{2(nmV_T)} \right) \quad (7)$$

where  $R_{ss} = V_{mp}/I_{mp}$  is the small-signal resistance at the MPP. This means that the power reduction due to ripple is greater than what would be predicted from the small-signal model by a factor  $(1 + \frac{V_{mp}}{2(nmV_T)})$ . For example, for typical values  $V_{mp} = 0.5$  V per cell,  $n = 1.4$ , and  $V_T = 26$  mV, this factor is about 7.87. This result is larger than expected from the linearized model because the curvature of the PV panel's  $I$ - $V$  curve contributes a second-order term to the power expression, in addition to the term that results from the first derivative of the  $I$ - $V$  curve, corresponding to the small-signal resistance.

The power reduction (7) can also be written as a fraction of power at the MPP  $(P_{mp})$  as follows:

$$\frac{P_r}{P_{mp}} \approx \left( \frac{(\Delta v)_{rms}}{V_{mp}} \right)^2 \left( 1 + \frac{V_{cell}}{2(nV_T)} \right) \quad (8)$$

where  $V_{cell}$  is the cell voltage at the MPP ( $V_{cell} = V_{mp}/m$ ). For the same parameter values used in the example above,  $P_r/P_{mp} \approx 7.87 ((\Delta v)_{rms}/V_{mp})^2$ , providing a very simple way to calculate the effect of ripple. For example, ripple with an rms amplitude equal to 8% of the MPP voltage would result in a 5% reduction in power output.

### A. Partial Shading

The analysis above is for a string of identical cells under identical irradiance. With mismatches in cell characteristics or in irradiance, the curvature of the  $I$ - $V$  characteristic at the MPP can become stronger, as shown, for example, in Fig. 2. Another example of this can be found in [23]. The strong curvature magnifies the effect of ripple. For an intuitive explanation of this effect, consider a string of 20 cells in series, and no bypass

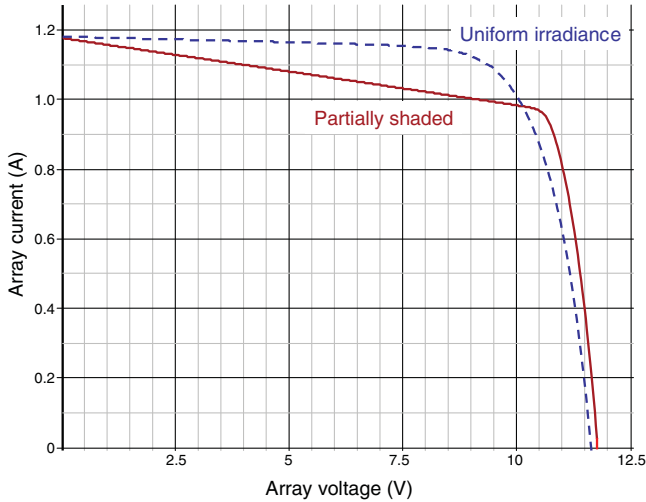


Fig. 2. Simulated  $V$ - $I$  curves for a solar panel with uniform irradiance and with partial shading on a small portion of the panel. The sharper corner at the MPP of the partially shaded panel leads to increased sensitivity to ripple. The model includes parallel resistance for each cell.

diodes. If most of the cells, under full irradiance, have a short-circuit current of 2 A, but one cell is shaded such that its short-circuit current is 1 A, then no cell can operate at more than 1 A. Thus, the majority of the cells will be operating near their open-circuit voltages, and can be crudely modeled as voltage sources. The MPP will be with a current very close to 1 A because, as current is increased up to 1 A, the voltage of most of the cells does not drop appreciably. Only the voltage of the one shaded cell changes significantly. Thus, the range of the voltage change for a significant change in current is compressed by a ratio approximately equal to the ratio of the number of unshaded cells to the number of shaded cells—a factor of 20 in our example. One can therefore expect that the effect of voltage ripple should also be magnified by about a factor of 20 compared to the case of uniform irradiance.

To analyze such situations, we write array voltage as a function of current  $v(i)$ , because each cell has the same current, and thus it is easier to get an explicit expression for voltage in terms of current. To find the effect of ripple, we will again use a Taylor expansion. Following steps analogous to (5)–(7), including noting that at the MPP, the first-order term drops out, leads to an analogous expression for the reduction in power

$$P_r \approx -\frac{1}{2} ((\Delta i)_{\text{rms}})^2 \frac{d^2 P}{di^2}. \quad (9)$$

This expression (9) is simply a different way of writing the same reduction in power described by (7).

The second derivative of power can be written as

$$\frac{d^2 P}{di^2} = 2 \frac{dv}{di} + i \frac{d^2 v}{di^2}. \quad (10)$$

The power reduction at the MPP  $I_{\text{mp}}$  is then

$$P_r \approx -((\Delta i)_{\text{rms}})^2 \left( \frac{dv}{di} + \frac{1}{2} I_{\text{mp}} \frac{d^2 v}{di^2} \right). \quad (11)$$

Appendix B works out these derivatives for a panel with  $m_a$  cells with a short-circuit current  $I_a$  and  $m_b$  cells with a short-circuit current  $I_b$ , assuming that all other parameters are the same for all cells. Substituting the derivatives into (11) results in

$$P_r \approx ((\Delta i)_{\text{rms}})^2 nV_T \left( \frac{m_a}{I_a + I_s - I_{\text{mp}}} + \frac{m_b}{I_b + I_s - I_{\text{mp}}} + \frac{I_{\text{mp}}}{2} \left( \frac{m_a}{(I_a + I_s - I_{\text{mp}})^2} + \frac{m_b}{(I_b + I_s - I_{\text{mp}})^2} \right) \right). \quad (12)$$

While (12) allows accurately calculating the power reduction, it provides little intuition. It also requires data on the short-circuit current of each cell (or the irradiance at each cell) which in practice might not be known. However, it is possible to gain some insight by focusing on the larger terms in the sum: with the  $a$  cells shaded, and thus with  $I_b$  significantly larger than  $I_a$ , the  $a$  cells will be operating much closer to their short-circuit current, and so their square terms will dominate. This means that the power reduction can be very roughly approximated as

$$P_r \approx ((\Delta i)_{\text{rms}})^2 m_a nV_T \frac{1}{2} \frac{I_{\text{mp}}}{(I_a + I_s - I_{\text{mp}})^2} \quad (13)$$

and applying similar approximations to write  $V_{\text{mp}} \approx nV_T m_a \frac{I_{\text{mp}}}{I_a + I_s - I_{\text{mp}}}$  (see Appendix B) and substituting leads to

$$P_r \approx ((\Delta i)_{\text{rms}})^2 \frac{V_{\text{mp}}}{2(I_a + I_s - I_{\text{mp}})} \approx ((\Delta i)_{\text{rms}})^2 R_{\text{ss}} \frac{V_{\text{mp}}}{2nm_a V_T} \quad (14)$$

In other words, the power reduction is greater than what would be expected based on the small-signal resistance by a factor  $\frac{V_{\text{mp}}}{2nm_a V_T}$ . This is very similar to the factor  $1 + \frac{V_{\text{mp}}}{2nm V_T}$  in (7), but our approximations have effectively dropped the 1, along with some other terms. However, even in (7), the factor  $\frac{V_{\text{mp}}}{2nm_a V_T} \gg 1$ , and the new factor for nonuniform radiation is significantly larger, if  $m_a$  is significantly less than  $m$ . In fact, neglecting the 1, the percentage power reduction due to ripple is, in the partial shading case, greater than in the uniform irradiance case, by a factor of approximately  $m/m_a$ . This is as expected based on the intuitive argument at the beginning of this section.

Precise calculations of theoretical reduction in power output due to ripple based on (11) for various numbers of shaded cells in a 40-cell string with different degrees of nonuniformity are shown in Fig. 3. The vertical axis of the plot is the ratio of power reduction calculated from (11) compared to the power reduction expected with uniform irradiance (7). This is the ratio that our approximate calculations predicted to be  $m/m_a$ , or, for the example in the plot,  $40/m_a$ . The figure shows that (14) gives a reasonable estimate as long as the shaded cells have significantly different irradiance than the nonshaded cells. It is also notable that the effect can be substantial even with mismatches of less than 10%, as can be seen more clearly in Fig. 4.

It is important to note that the approximation of using only the second-order terms in the Taylor expansion will be less accurate with very sharp corners in the  $I$ - $V$  curve. Thus, as ripple gets large, these approximations lose accuracy faster than those for uniform irradiance, which are approximating a smoother curve.

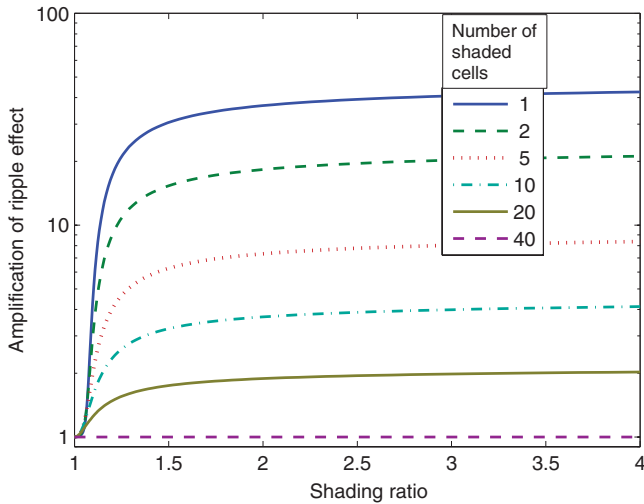


Fig. 3. Calculated reduction in power output due to ripple under partial shading compared to that with uniform irradiance for a series string of cells. The shading ratio of the horizontal axis is defined as the ratio of insolation on the unshaded cells to insolation on the shaded cells. The vertical axis is the ratio of power reduction calculated from (11) compared to the power reduction expected with uniform irradiance (7). The legend shows the number of shaded cells  $m_a$  in a string of 40. Cell parameters are  $n = 1.4$ ,  $V_T = 26$  mV, and  $I_s = 73.5$  nA. The shaded cells have a short-circuit current of 1 A, which results in a MPP voltage of 0.5 V.

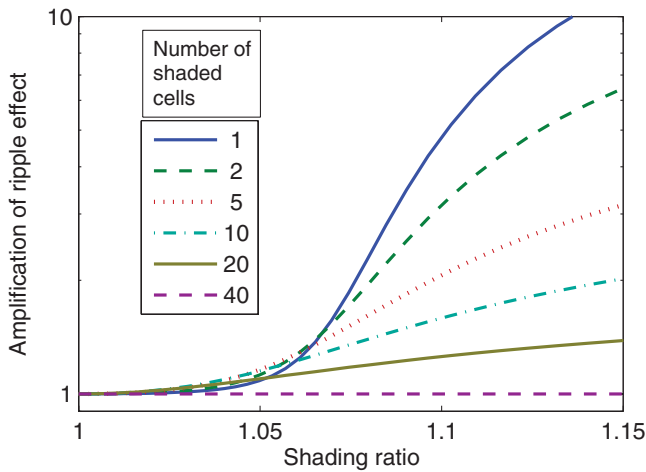


Fig. 4. Zoomed-in view of the same calculated reduction in power output shown in Fig. 3, showing that even a small mismatch caused by partial shading (e.g., 10%) can make the effect of ripple many times larger than with uniform irradiance.

The analysis above and the plot are only for the case of two different levels of irradiance. In the general case, the result is dominated by the most weakly irradiated cell or group of cells, and the effect of ripple will be similarly magnified, approximately inversely proportional to the number of cells in this group.

Cases with bypass diodes may be addressed by separately considering operation at local maxima with a particular diode on or off. With the diode ON, those cells do not participate, and the analysis above can be applied with  $m$  equal to the number of active cells not bypassed by the diode. With the diode OFF, the diode has no significant effect and the analysis above applies directly.

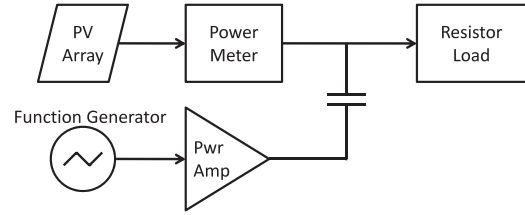


Fig. 5. Test setup for measuring the effect of ripple. Not shown is a multimeter used to monitor rms ripple voltage, light source (solar or artificial), and cooling fan.

### III. EXPERIMENTAL VERIFICATION

To test the analysis in Section II, we artificially added ripple with various waveforms, amplitudes, and frequencies to a small single-crystal Si PV panel and measured the effect on power output. The apparatus used is shown in Fig. 5. The PV panel (Sunwize SC6-12) was connected to a variable-resistor load through a Voltech PM6000 power analyzer configured with a 10-MHz-bandwidth shunt with a 1-A nominal current rating. A function generator was fed through a Hafler P4000 amplifier and a 60-mF capacitor to apply an ac voltage perturbation with control of the frequency, amplitude, and waveform. Although the power amplifier may source some power in addition to that sourced by the panel, the position of the power meter ensures measurement of the power output of the panel itself. The ripple frequencies tested (up to 30 kHz) are well below the 10-MHz bandwidth of the power analyzer, ensuring accurate measurements with ripple. Rms ripple amplitude is measured with an Agilent 34401A multimeter with 300-kHz bandwidth. A fan directed airflow across the panel in order to reduce the thermal time constant and reach steady-state temperature operation more rapidly.

Most tests used tungsten-halogen lamps as the light source. The lamps were powered from a dc source to eliminate ripple in the irradiance after initial tests with the lamp supplied from 60-Hz ac power showed substantial ripple.

The test procedure starts with the waveform generator output disabled. The panel is placed in the sun or under the halogen lamp, and a resistive load is manually adjusted to find the approximate MPP. The panel temperature is allowed to stabilize. The load is then carefully adjusted to find the MPP. Next, for each ripple signal tested, the signal generator output is switched on and off and the panel output power is recorded for both conditions. The difference between these readings is the power reduction associated with the ripple amplitude applied.

The experiments with tungsten-halogen irradiation (see Fig. 6) were more tightly controlled and repeatable than the experiments with solar irradiation (see Fig. 9). Thus, these experiments were used to more carefully examine the behavior with different ripple waveforms, frequencies, and amplitudes. These data are collected in Fig. 6, along with predicted power reduction based on (7) and based on the naive small-signal model. For (7), the value of  $nV_T$  (product of nonideality coefficient and thermal voltage) was found to be 29.28 mV from fitting the model to an experimental  $I$ - $V$  curve. At the MPP with no ripple, power output was about 1.25 W.

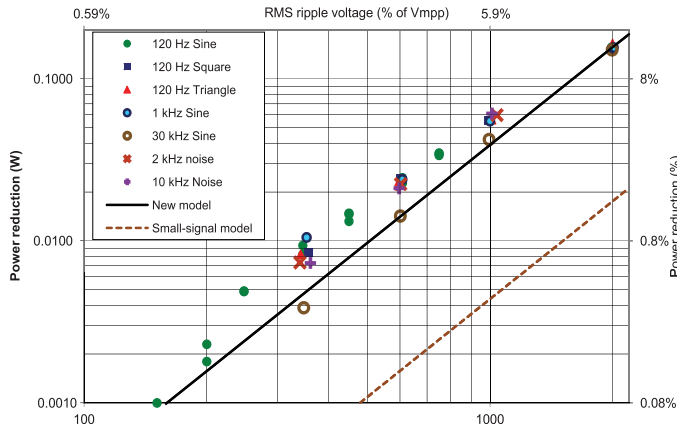


Fig. 6. Experimentally measured power reduction as a function of the rms amplitude of the ripple voltage for various waveforms and frequencies under uniform artificial tungsten-halogen irradiation, compared to calculated power reduction. The noise experiments used wideband Gaussian noise filtered with a simple  $RC$  filter with the indicated cutoff frequency. With no ripple, the MPP voltage, current, and power were 16.9 V, 73.9 mA, and 1.25 W, respectively. Short-circuit current was 77.8 mA, and open-circuit voltage 19.85 V.

The new model (7) can be seen in Fig. 6 to be a much closer match to the data than the naive small-signal model. At 2-V rms ripple, the data for all of the different periodic waveforms and frequencies are nearly identical, and coincides very closely with the model, with average error of only 3.8 mW, which is 1.4% of the predicted power reduction and 0.3% of the MPP power. This confirms that the model works well, and also confirms that the rms amplitude of the ripple is what matters, independent of waveform. As the ripple amplitude is reduced, the data get noisier, as expected, because it becomes harder to measure the smaller power reductions precisely. There does, however, appear to be some systematic error, with the actual ripple reduction often significantly higher than the prediction (note the log scale in the plot). This is most likely a result of imperfect uniformity of irradiance, as discussed in Section II-A. Again, the data for different waveforms and frequencies are consistent, including noise waveforms (for which data are only available up to 1-V rms amplitude), but with the possible exception of the 30-kHz ripple. Although the 30-kHz data are consistent with the model, the loss reduction appears to be systematically lower for 30 kHz. We believe that this is a result of cell capacitance improving the division of ripple voltage between cells, and thus mitigating the effect of partial shading on ripple sensitivity. Other possible, but less likely, reasons for the smaller decrease in power at 30 kHz include stray coupling of additional signal into the meter used to measure ripple amplitude, or reduced amplitude ripple on the cells themselves due to filtering created by wiring to the cells and the cells' capacitance.

Initial results before we took care to set up a system with approximately uniform irradiance on the panel are shown in Fig. 7, demonstrating reduction of power output much larger than predicted from (7), consistent with the analysis in Section II-A. This is corroborated by the similarity of shape of the experimental  $I$ - $V$  curve shown in Fig. 8 to the shape of the simulated curve in Fig. 2.

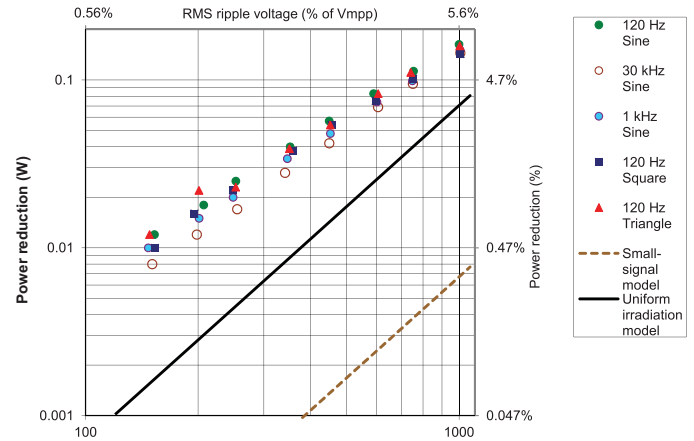


Fig. 7. Experimentally measured power reduction as a function of the rms amplitude of the ripple voltage for various waveforms and frequencies under nonuniform irradiance, compared to calculated power reduction for uniform irradiance. With no ripple, the MPP voltage, current, and power were 17.8 V, 119.5 mA, and 2.13 W, respectively. Short-circuit current was 132 mA, and open-circuit voltage 19.7 V.

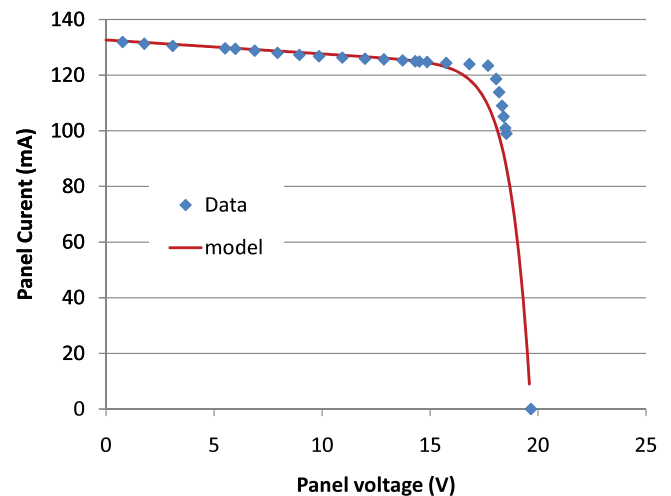


Fig. 8. Experimental  $I$ - $V$  curve for the panel under nonuniform artificial irradiation, compared to a model with nonideality coefficient  $n = 1$  and a parallel resistance of 2 k $\Omega$ . The sharper corner of the experimental curve indicates nonuniform irradiance, as in one of the curves in Fig. 2.

Results for tests with solar irradiation are shown in Fig. 9. The data are shown only for relatively large ripple of 1-V rms, because temporal variations in irradiance were greater than the effect of the ripple, making it hard to collect meaningful data with small ripple, even on an apparently cloudless day. The model predicts the power reduction very accurately, considering the difficulty in collecting data under naturally varying irradiance. Note that the difference in predicted power reduction with different waveforms does not reflect differences in the effect of those waveforms—rather it represents the different temperature and irradiance conditions when each data point was collected. Power output at the MPP ranged from 1.6 to 3.6 W in these experiments. The results did not suffer from the systematic increase in ripple sensitivity found in Fig. 6 and especially Fig. 7. As the tests with solar irradiation had highly uniform

TABLE 1  
DETAILS OF EXPERIMENTAL MEASUREMENTS UNDER SOLAR IRRADIATION, INCLUDING OPERATION WITHOUT RIPPLE  
AND POWER REDUCTION WITH 1-V rms RIPPLE.

Ripple waveform	Without Ripple					With Ripple				
	Maximum power point			Open cir. vltg. (V)	Short cir. curr. (mA)	Power reduction (mW)				Ripple voltage in % (all 1 V rms)
	Voltage (V)	Current (mA)	Power (W)			Predicted with R <sub>ss</sub>	Pred. with new model	Meas.	Meas. (%)	
120 Hz Square	14.7	197	2.89	19.7	199	13.4	76.5	101.0	3.5%	6.8%
120 Hz Triangle	15.4	221	3.40	19.7	228	14.4	85.4	89.5	2.6%	6.5%
120 Hz Sine	15.4	235	3.63	19.7	243	15.3	90.7	70.0	1.9%	6.5%
30 kHz Sine	14.5	110	1.59	19.7	142	7.6	42.9	38.0	2.4%	6.9%
1 kHz Sine	14.5	141	2.06	19.8	112	9.7	55.1	56.5	2.7%	6.9%

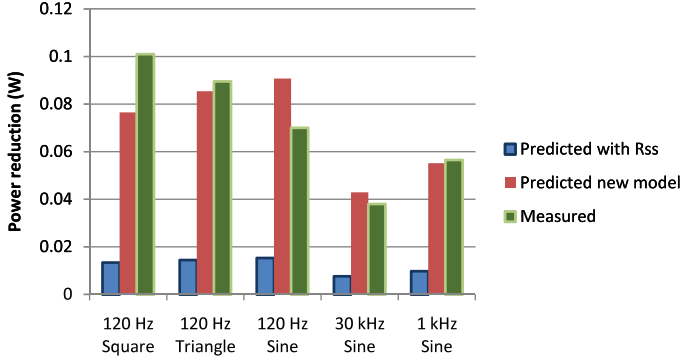


Fig. 9. Experimentally measured power reduction with 1 V rms ripple amplitude under solar irradiation, compared to predictions. Note that the difference in predicted power reduction with different waveforms does not reflect differences in the effect of those waveforms—rather it represents the different temperature and irradiance conditions when each data point was collected. Details are in Table I

irradiance on the panel, this is consistent with our attribution of the discrepancies in Figs. 6 and 7 to nonuniform irradiance.

#### IV. CONCLUSION

The power reduction resulting from ripple is much greater than would be predicted from a small-signal model. Under uniform irradiance, it can be simply estimated from rms ripple voltage using (8). Under nonuniform irradiance (e.g., partial shading), it can be significantly higher. These results apply to all of the various types of ripple a solar panel may be subjected to, including double-line-frequency ripple in single-phase inverters, high-frequency switching ripple with any switching power converter, and perturbations and tracking errors in MPPT systems.

#### APPENDIX A

##### DERIVATIVES FOR UNIFORM IRRADIANCE OR SINGLE CELLS

Consider a cell, or string of  $m$  identical cells, operating at the MPP. At the MPP  $\frac{dP}{dv} = 0$ . The derivative, in terms of any panel characteristic  $i(v)$ , is

$$\frac{dP}{dv} = v \frac{di}{dv} + i \quad (15)$$

and so

$$0 = V_{mp} \frac{di}{dv} + I_{mp}. \quad (16)$$

Thus, at the MPP,  $\frac{di}{dv} = -\frac{I_{mp}}{V_{mp}}$ , and thus the small-signal resistance  $R_{ss}$  at the MPP is

$$R_{ss} = \frac{V_{mp}}{I_{mp}}. \quad (17)$$

(The minus sign is dropped because we have defined polarities consistent with positive power flow out of the cell.)

Now consider derivatives of power based on the exponential cell model, starting with the power for a panel (3)

$$P = v(t)I_{sc} - v(t)I_s \left( e^{\frac{v(t)}{nmV_T}} - 1 \right). \quad (18)$$

The next step is to take the first derivative

$$\frac{dP}{dv} = I_{sc} - I_s \left( e^{\frac{v}{nmV_T}} - 1 \right) - vI_s \frac{1}{nmV_T} e^{\frac{v}{nmV_T}} \quad (19)$$

and the second derivative

$$\begin{aligned} \frac{d^2P}{dv^2} &= \left( -I_s \frac{1}{nmV_T} - I_s \frac{1}{nmV_T} - vI_s \frac{1}{(nmV_T)^2} \right) e^{\frac{v}{nmV_T}} \\ &= -2I_s \frac{1}{nmV_T} e^{\frac{v}{nmV_T}} - vI_s \frac{1}{(nmV_T)^2} e^{\frac{v}{nmV_T}}. \end{aligned} \quad (20)$$

At the MPP, the first derivative is zero, and so

$$I_{sc} - I_s \left( e^{\frac{V_{mp}}{nmV_T}} - 1 \right) = I_{mp} = V_{mp} I_s \frac{1}{nmV_T} e^{\frac{V_{mp}}{nmV_T}}. \quad (21)$$

Using (17)

$$\frac{1}{R_{ss}} = \frac{I_{mp}}{V_{mp}} = I_s \frac{1}{nmV_T} e^{\frac{V_{mp}}{nmV_T}}. \quad (22)$$

Substituting (22) into (20) leads to

$$\frac{d^2P}{dV^2} = -\frac{2}{R_{ss}} - \frac{V_{mp}}{(nmV_T)R_{ss}} \quad (23)$$

This, used in (6), yields (7).

#### APPENDIX B

##### CALCULATIONS FOR NONUNIFORM IRRADIANCE

Consider a panel with  $m_a$  cells with a short-circuit current  $I_a$  and  $m_b$  cells with a short-circuit current  $I_b$ . For simplicity, we assume that all other parameters are the same for all cells. The voltage as a function of current is

$$v(i) = m_a n V_T \ln \left( \frac{I_s + I_a - i}{I_s} \right) + m_b n V_T \ln \left( \frac{I_s + I_b - i}{I_s} \right) \quad (24)$$

and its first and second derivatives are

$$\frac{dv}{di} = -nV_T \left( \frac{m_a}{I_a + I_s - i} + \frac{m_b}{I_b + I_s - i} \right) \quad (25)$$

and

$$\frac{d^2v}{di^2} = -nV_T \left( \frac{m_a}{(I_a + I_s - i)^2} + \frac{m_b}{(I_b + I_s - i)^2} \right). \quad (26)$$

Plugging those values into (11) results in

$$P_r \approx ((\Delta i)_{\text{rms}})^2 nV_T \left( \frac{m_a}{I_a + I_s - I_{\text{mp}}} + \frac{m_b}{I_b + I_s - I_{\text{mp}}} + \frac{I_{\text{mp}}}{2} \left( \frac{m_a}{(I_a + I_s - I_{\text{mp}})^2} + \frac{m_b}{(I_b + I_s - I_{\text{mp}})^2} \right) \right). \quad (27)$$

A simplified approximation for this expression is discussed in Section II-A. For this purpose, it is useful to write an approximate expression for the MPP voltage. At the MPP, the first derivative of power,  $\frac{dP}{di} = i \frac{dv}{di} + v = 0$ , and so

$$V_{\text{mp}} = -I_{\text{mp}} \frac{dv}{di} = I_{\text{mp}} nV_T \left( \frac{m_a}{I_a + I_s - I_{\text{mp}}} + \frac{m_b}{I_b + I_s - I_{\text{mp}}} \right). \quad (28)$$

As discussed in Section II-A, for  $I_a$  significantly less than  $I_b$ ,  $I_{\text{mp}}$  is much closer to  $I_a$  than to  $I_b$ . As a result, the first fraction dominates this expression, even if  $m_a$  is smaller than  $m_b$ , and it is a good approximation to write

$$V_{\text{mp}} \approx nV_T m_a \frac{I_{\text{mp}}}{I_a + I_s - I_{\text{mp}}}. \quad (29)$$

## REFERENCES

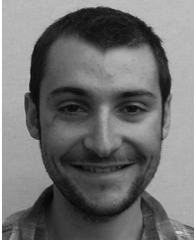
- [1] T. Esram and P. L. Chapman, "Comparison of photovoltaic array maximum power point tracking techniques," *IEEE Trans. Energy Convers.*, vol. 22, no. 2, pp. 439–449, Jun. 2007.
- [2] V. Salas, E. Olías, A. Barrado, and A. Lázaro. (2006). Review of the maximum power point tracking algorithms for stand-alone photovoltaic systems. *Solar Energy Mater. Solar Cells* [Online]. 90(11), pp. 1555–1578. Available: <http://www.sciencedirect.com/science/article/B6V51-4J0WRC7-2/2/ace7c72150a4c9afbd031d258c2cf201>
- [3] S. Kjaer, J. Pedersen, and F. Blaabjerg, "A review of single-phase grid-connected inverters for photovoltaic modules," *IEEE Trans. Ind. Appl.*, vol. 41, no. 5, pp. 1292–1306, Sep./Oct. 2005.
- [4] P. Krein and R. Balog, "Cost-effective hundred-year life for single-phase inverters and rectifiers in solar and led lighting applications based on minimum capacitance requirements and a ripple power port," in *Proc. IEEE Appl. Power Electron. Conf.*, 2009, pp. 620–625.
- [5] S. Brunton, C. Rowley, S. Kulkarni, and C. Clarkson, "Maximum power point tracking for photovoltaic optimization using ripple-based extremum seeking control," *IEEE Trans. Power Electron.*, vol. 25, no. 10, pp. 2531–2540, Oct. 2010.
- [6] M. Joshi, E. Shoubaki, R. Amarín, B. Modick, and J. Enslin, "A high-efficiency resonant solar micro-inverter," in *Proc. 14th Eur. Conf. Power Electron. Appl.*, pp. 1–10.
- [7] T.-F. Wu, C.-H. Chang, L.-C. Lin, and C.-L. Kuo, "Power loss comparison of single- and two-stage grid-connected photovoltaic systems," *IEEE Trans. Energy Convers.*, vol. 26, no. 2, pp. 707–715, Jun. 2011.
- [8] G. Ertasgin, D. Whaley, N. Ertugrul, and W. Soong, "Analysis and design of energy storage for current-source 1-ph grid-connected PV inverters," in *IEEE Appl. Power Electron. Conf.*, 2008, pp. 1229–1234.
- [9] D. Casadei, G. Grandi, and C. Rossi, "Single-phase single-stage photovoltaic generation system based on a ripple correlation control maximum power point tracking," *IEEE Trans. Energy Convers.*, vol. 21, no. 2, pp. 562–568, Jun. 2006.
- [10] K. H. Edelmoser and F. A. Himmelstoss, "A simple, efficient, and EMI-optimized solar array inverter," *WSEAS Trans. Circuits Syst.*, vol. 9, no. 9, pp. 597–606, 2010.
- [11] P. T. Krein, R. S. Balog, and M. Mirjafari, "Minimum energy and capacitance requirements for single-phase inverters and rectifiers using a ripple port," *IEEE Trans. Power Electron.*, vol. 27, no. 11, pp. 4690–4698, Nov. 2012.
- [12] K. Ishaque, Z. Salam, M. Amjad, and S. Mekhilef, "An improved particle swarm optimization (PSO)-based MPPT for PV with reduced steady state oscillation," *IEEE Trans. Power Electron.*, vol. 27, no. 8, pp. 3627–3638, 2012.
- [13] A. M. Latham and C. R. Sullivan, "Optimization of a continuous-time maximum power point tracking algorithm in the presence of noise," in *Proc. 12th IEEE Workshop Control Modeling Power Electron.*, Jun. 2010, pp. 1–7.
- [14] A. Latham, C. Sullivan, and K. Odame, "Performance of photovoltaic maximum power point tracking algorithms in the presence of noise," in *Proc. IEEE Energy Convers. Congr. Expo.*, Sep. 2010, pp. 632–639.
- [15] S. B. Kjaer. (2004/2005). "Design and control of an inverter for photovoltaic applications," Ph.D. dissertation, Inst. Energy Technol., Aalborg University, Aalborg East, Denmark, [Online]. Available: [http://vbn.aau.dk/da/publications/design-and-control-of-an-inverter-for-photovoltaic-applications\(49b33310-7204-11de-9240-000ea68e967b\).html](http://vbn.aau.dk/da/publications/design-and-control-of-an-inverter-for-photovoltaic-applications(49b33310-7204-11de-9240-000ea68e967b).html).
- [16] N. D. Benavides and P. L. Chapman, "Modeling the effect of voltage ripple on the power output of photovoltaic modules," *IEEE Trans. Ind. Electron.*, vol. 55, no. 7, pp. 2638–2643, Jul. 2008.
- [17] C. Sullivan, J. Awerbuch, and A. Latham, "Decrease in photovoltaic power output from ripple: Simple general calculation and effect of partial shading," in *Proc. IEEE Appl. Power Electron. Conf. Expo.*, 2011, pp. 1954–1960.
- [18] T. Esram, J. W. Kimball, P. T. Krein, P. L. Chapman, and P. Midya, "Dynamic maximum power point tracking of photovoltaic arrays using ripple correlation control," *IEEE Trans. Power Electron.*, vol. 21, no. 5, pp. 1282–1291, Sep. 2006.
- [19] J. Kimball and P. T. Krein, "Discrete-time ripple correlation control for maximum power point tracking," *IEEE Trans. Power Electron.*, vol. 23, no. 5, pp. 2353–2362, Sep. 2008.
- [20] A. Bazzi and P. Krein, "Correspondence concerning maximum power point tracking for photovoltaic optimization using ripple-based extremum seeking control," *IEEE Trans. Power Electron.*, vol. 26, no. 6, pp. 1611–1612, Jun. 2011.
- [21] M. Villalva, J. Gazoli, and E. Filho, "Comprehensive approach to modeling and simulation of photovoltaic arrays," *IEEE Trans. Power Electron.*, vol. 24, no. 5, pp. 1198–1208, May 2009.
- [22] S. Liu and R. Dougal, "Dynamic multiphysics model for solar array," *IEEE Trans. Energy Convers.*, vol. 17, no. 2, pp. 285–294, Jun. 2002.
- [23] K. Wilson, D. D. Ceuster, and R. A. Sinton, "Measuring the effect of cell mismatch on module output," in *Proc. IEEE 4th World Conf. Photovolt. Energy Convers.*, May 2006, pp. 916–919.



**Charles R. Sullivan** (SM'93–M'96–SM'12) received the B.S. degree in electrical engineering (with highest Hons.) from Princeton University, Princeton, NJ, in 1987, and the Ph.D. degree in electrical engineering from the University of California, Berkeley, in 1996.

He is currently an Associate Professor at the Thayer School of Engineering at Dartmouth, Hanover, NH. He worked for Lutron Electronics designing electronic ballasts. His research includes work on design optimization of magnetics for high-frequency power conversion, thin-film magnetic materials and devices, and photovoltaic applications of power electronics.

Dr. Sullivan has received the National Science Foundation Career Award and the Power Electronics Society Prize Paper Award.



**Jonathan J. Awerbuch** received the A.B. degree in engineering sciences and the M.S. degree in mechanical engineering from Dartmouth College, Hanover, NH, in 2007 and 2009, respectively, the M.E. degree from Yale University, New Haven, CT, in 2010; and is now working toward the Ph.D. degree at the University of Colorado, Boulder.

His current research at the University of Colorado considers high-efficiency construction and its impact on indoor air quality. His past publications and research include power electronic and ultracapacitor systems to improve electric vehicle efficiency, photovoltaic performance, and energy efficient electrothermal heaters.



**Alexander M. Latham** (M'09) was born in Boston, MA, on October 18, 1986. He received the A.B. degree (*summa cum laude*) at Dartmouth College, Hanover, NH, in 2009. He went on to complete the B.E. and M.S. degrees in electrical engineering at the Thayer School of Engineering at Dartmouth, Hanover, NH, graduating in 2011.

His research while at Dartmouth focused on the optimization of power electronics and system level algorithms for power extraction from photovoltaics. He currently works as a Systems Engineer at Allegro Microsystems in Manchester, NH, developing Hall-effect-based current and position sensor ASICs.